

# Ambient seismic noise in an urban environment: case study using downhole distributed acoustic sensors at the Curtin University campus in Perth, Western Australia

Valeriya Shulakova, Konstantin Tertyshnikov, Roman Pevzner, Yevhen Kovalyshen & Boris Gurevich

To cite this article: Valeriya Shulakova, Konstantin Tertyshnikov, Roman Pevzner, Yevhen Kovalyshen & Boris Gurevich (2022): Ambient seismic noise in an urban environment: case study using downhole distributed acoustic sensors at the Curtin University campus in Perth, Western Australia, Exploration Geophysics, DOI: [10.1080/08123985.2021.2021802](https://doi.org/10.1080/08123985.2021.2021802)

To link to this article: <https://doi.org/10.1080/08123985.2021.2021802>



Published online: 24 Jan 2022.



Submit your article to this journal [↗](#)



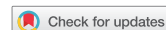
Article views: 61



View related articles [↗](#)



View Crossmark data [↗](#)



# Ambient seismic noise in an urban environment: case study using downhole distributed acoustic sensors at the Curtin University campus in Perth, Western Australia

Valeriya Shulakova<sup>a</sup>, Konstantin Tertyshnikov<sup>b</sup>, Roman Pevzner<sup>b</sup>, Yevhen Kovalyshen<sup>a</sup> and Boris Gurevich<sup>b</sup>

<sup>a</sup>CSIRO Energy, Perth, Australia; <sup>b</sup>Centre for Exploration Geophysics, Curtin University, Perth, Western Australia

## ABSTRACT

Distributed acoustic sensing (DAS) is an emerging technology increasingly employed to monitor changes of formation properties, production noise and micro-seismic activity, and as an array of sensors in active seismic surveys. The data recorded with the DAS systems are very rich; some features observed in DAS records are often not well understood, and thus are underutilised. A systematic analysis of the data recorded passively with a DAS system in a 900-m deep well over a period of 12 weeks in the Perth metropolitan area, Western Australia, reveals the presence of several types of ambient energy in the subsurface, such as earthquakes, ocean swell and urban noise. In particular, over 85 days of the experiment, the analysis detected sixteen earthquakes, with epicentres ranging from 126 km to 900 km (for the local events) and from 2300 km to 6400 km (for the remote events). Signals with frequencies below 0.9 Hz are dominated by the oceanic swell. The recorded urban noise includes mine blasting, machinery and traffic. The experiment shows the ability of DAS to detect these events and as such is potentially useful for subsurface characterisation and monitoring.

## ARTICLE HISTORY

Received 13 April 2021  
Accepted 19 December 2021

## KEYWORDS

Remote sensing; passive; monitoring; borehole geophysics; characterisation; noise

## Introduction

Distributed acoustic sensing (DAS) is a novel sensing technology for active and passive seismic monitoring and characterisation. A central element of a DAS system is an interrogator, which sends a pulse down an optical fibre and records back-scattered light (Hartog 2017). DAS uses an optical fibre itself as a sensing element. As such, the DAS technology allows the deployment of large arrays of seismic sensors to virtually any location on or under the Earth surface, providing a dense spatial and temporal sampling of recorded signals (Hartog 2020).

DAS technology allows a cost-effective installation of highly sensitive dense arrays of acoustic receivers, which can record seismic waves in a broad frequency band. At the lower end of the frequency spectrum, DAS can measure strain in the mHz range (Parker, Shatalin, and Farhadiroushan 2014; Becker et al. 2017). The upper-frequency limit of DAS is defined by the Nyquist frequency, which is in the range of tens of kHz. An optical fibre is naturally unaffected by corrosion over time, which is important for reliable long-term monitoring when deployed underground. One example of long-term DAS deployment comes from the San Andreas Fault Observatory at Depth, where a fibre was used for twelve years (Lellouch et al. 2019a).

High sensitivity, high spatial sampling, broad bandwidth, relatively low cost as well as resistance to high temperatures and corrosion, and excellent repeatability (Daley et al. 2013) make the use of DAS in seismic monitoring a rapidly developing area (Lellouch and Biondi 2021).

The DAS technology has been applied to various seismic studies including monitoring of naturally occurring events as well as human-related everyday activities and exploration studies. Several recent studies report the application of distributed acoustic sensing in global seismology (Lellouch et al. 2019b; Biondi et al. 2017; Ajo-Franklin et al. 2019; Yu et al. 2019). Lindsey et al. (2017) analysed regional/teleseismic earthquake waveforms from three different DAS arrays in Alaska, and California. Wang et al. (2018) found coherent earthquake waveforms recorded at a dense DAS array and a dense geophone array from a local ML4.3 event. Lellouch et al. (2021) used DAS to study seismicity around the FORGE Enhanced Geothermal System experiment. Using a downhole DAS array, they recorded low-magnitude earthquakes at a range of up to 10 km from the well location. Hudson et al. (2021) and Walter et al. (2020) reported applications of the DAS technology to monitor icequakes in Antarctica and the Alpine mountain glacier, respectively. Williams et al. (2019)

and Glubokovskikh et al. (2020) utilised DAS to study oceanic microseisms, while Martin et al. (2016) used DAS to monitor permafrost thaw.

Another popular application of DAS is monitoring human activity. Unused telecommunications fibre enables easy access to many urban locations (Lindsey and Martin Eileen 2021). In particular, Shen and Zhu (2021) showed how the use of telecommunication fibre aids in quantifying human activities during COVID-19 pandemic measures. There are many examples of using DAS for perimeter monitoring and security applications or characterising traffic patterns (see e.g. Martin et al. 2017). Dou et al. (2017) used traffic noise interferometry for seismic monitoring of the near-surface structure.

Nowadays DAS is frequently applied in resource exploration. In particular, DAS is rapidly being adapted in Vertical Seismic Profiling (VSP) acquisitions, particularly in wells inaccessible for geophones (Mestayer et al. 2011; Mateeva et al. 2012). The DAS technology has also been utilised for passive seismic studies including monitoring of hydrocarbon production and CO<sub>2</sub> geo-sequestration (Daley et al. 2013), monitoring hydraulic fracture reservoir stimulation (Verdon et al. 2020; Richter et al. 2019) and microseismic monitoring on geothermal sites (Mondanos and Coleman 2019).

One advantage of DAS is the ability to install and use it in urban settings. Stanford DAS array in California was installed in existing telecommunications conduits under the Stanford University campus (Martin et al. 2017a). That array was used for ambient noise interferometry (Martin et al. 2017b), earthquake detection (Biondi et al. 2017), urban seismic site characterisation (Spica et al. 2020) and active seismic survey recording. Another example is 460-m deep Houston Aramco Research Centre Test Well used for a series of studies to evaluate various aspects of DAS acquisition technology, such as comparison to geophones and influence of gauge length on VSP data quality (Alfataierge et al. 2020).

The ambient seismic energy propagating in the subsurface can come from various sources such as earthquakes, other natural powers like the ocean, and human-related activities (especially in an urban environment). The use of this ambient energy as a seismic source could potentially lead to a reduction of the cost of seismic acquisition, its environmental footprint and disturbance to other land users. A number of studies demonstrate the feasibility of this approach (Issa, Lumley, and Pevzner 2017), and its uses (Dou et al. 2017). Shragge et al. (2019) analysed a low-frequency swell signal recorded on a DAS array using a combination of seismic interferometry and multi-channel analysis of surface waves (MASW) to estimate a 1D S-wave velocity profile down to a depth of 750 m. Studies conducted at the Stanford DAS array facility with a horizontal fibre showed the potential of the ambient noise seismic interferometry (Martin and Biondi 2018).

Passive downhole DAS acquisition was trialled in several wells in Australia, including wells located in rural Victoria (Glubokovskikh et al. 2021) and rural Western Australia (Pevzner et al. 2020). Unlike near-surface studies mentioned above, downhole data are much less affected by ground roll, which gives an advantage in the analysis of body waves and their sources. Despite some similarities, the distribution of the dominant ambient noise sources and the methods which can be utilised to retrieve the information about the subsurface are site specific. Therefore, further studies utilising DAS acquisition for passive seismic recording in different parts of the world and different environments are in order.

The paper focuses on the passive DAS data acquired continuously in a vertical 900-m deep well located in an urban setting at the Curtin University campus in Perth, Western Australia. There is a limited number of deep wells drilled in cities, and to our knowledge, this is the only such well where long continuous passive seismic recording using DAS is available. A pilot attempt to collect passive data in the Curtin well was in 2018 (Pevzner, Tertyshnikov, and Bona 2018) and lasted for one day. Analysis of these data revealed the presence of a significant number of surface seismic events originating at distances of up to several hundred metres from the well, predominantly arising from human activities. Pevzner, Tertyshnikov, and Bona (2018) also found that there is an advantage in individual event analysis over conventional passive seismic interferometry. However, in order to fully characterise the passive seismic field, a longer acquisition is needed. In this paper, we analyse the data from the same well, covering nearly three months of acquisition. By using spectral analysis and kinematics of the recorded seismic waves, we identify a number of different sources, both anthropogenic and natural.

## Data acquisition

The passive seismic data were acquired using distributed acoustic sensing (DAS) system at the Curtin NGL training well in Bentley, Western Australia (Figure 1). The well is located 13 km away from the Indian Ocean coast, in the middle of the student campus close to busy roads. The data were recorded continuously from 16 May 2018 till 9 August 2018, totalling 85 days of recordings in total.

The well is 900 m deep and instrumented with a fibre-optic cable cemented behind the fibreglass casing of the 152/180 mm inside/outside diameter. The casing is machine slotted below 652 m with 1.3–1.45 mm aperture. The armoured non-metallic cable is deployed to a total depth of 900 m and physically looped at the bottom. It carries four multi-mode ( $2 \times 62.5 \mu\text{m}$  OM1 and  $2 \times 50 \mu\text{m}$  OM2) and two single-mode optical fibres ( $2 \times \text{G.652d SM}$ ). The seismic acquisition parameters were as follows: 18.5 m gauge length, 12.3 m pulse length and 30 kHz pulse repetition frequency. The data set

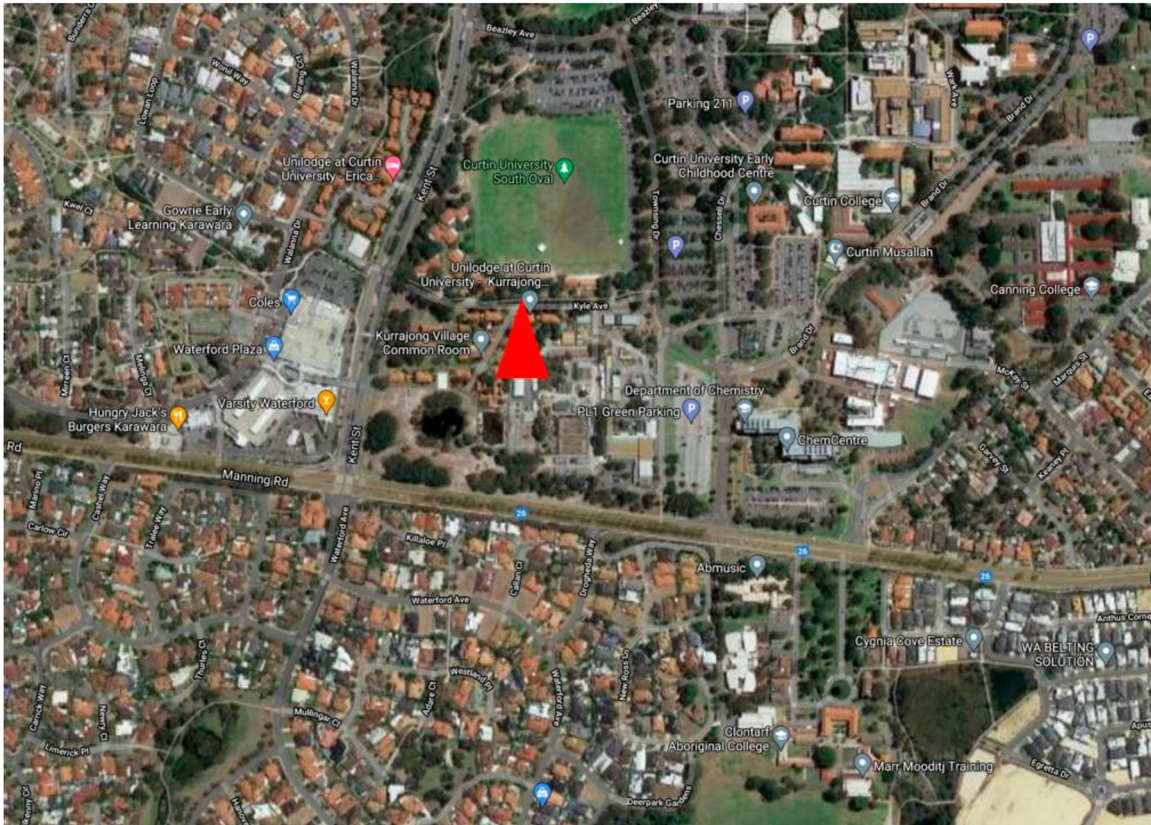


**Figure 1.** Curtin NGL training well location (marked with a red triangle) in Bentley, Western Australia.

was acquired using the Fotech Helios Theta dual pulse true phase interrogator unit and one of the single-mode fibres. Fotech Helios Theta measures the so-called dynamic strain expressed as a phase change in radians. The vertical channel spacing was 0.67 m. The data set was later resampled to 5 m/4 ms space/time sampling for further processing. The volume of the resampled data set is 1338 GB.

## Data analysis

DAS has a significant sensitivity within a broad frequency range; as a result, the recorded passive data have very rich content in terms of the presence of a vast number of various seismic events. Many major events, like distant and local earthquakes, as well as local mine blasting, are directly visible on the seismograms.

In order to thoroughly inspect the acquired data set and detect and describe diverse seismic occurrences, we analysed data in several domains. First, we examined the data in the time–depth domain, which is a native format of the acquired seismograms. The analysis provides information on the individual components of the wavefield and allows their detection and separation using travel–time curves.

Another powerful approach to explore DAS data is creating spectrograms by decomposing data to the time–frequency domain. This spectrogram analysis gives us overall information about the wave field

and distribution of events throughout the recorded frequency range. The spectrograms show the contribution of human activity (traffic, machinery) and the natural events (such as the ocean swell) to the total wavefield as well as variations and evolution of these contributions over time. The data analysis reveals and allows an analysis of different wavefield components initiated by natural (e.g. oceans) and anthropogenic sources (e.g. mine blasting).

## Results

Here, we categorise and describe the detected events in detail.

### *Regional and distant earthquakes*

When an earthquake occurs, it generates large amounts of energy that transmits as compressional and shear waves, which are detectable by DAS sensors. Due to the systematic increase of velocities with depth, body waves from remote sources such as earthquakes propagate as head waves or diving waves, and thus arrive at the surface almost vertically, and hence travel along the fibre with the apparent velocity close to the interval velocity. Thus, all earthquakes have a distinct pattern on the downhole DAS data, comprising a set of upgoing waves (see Figure 2). Compressional or P-wave arrivals arrive first and are usually clearly visible on borehole DAS seismograms. Shear or S-wave arrivals are

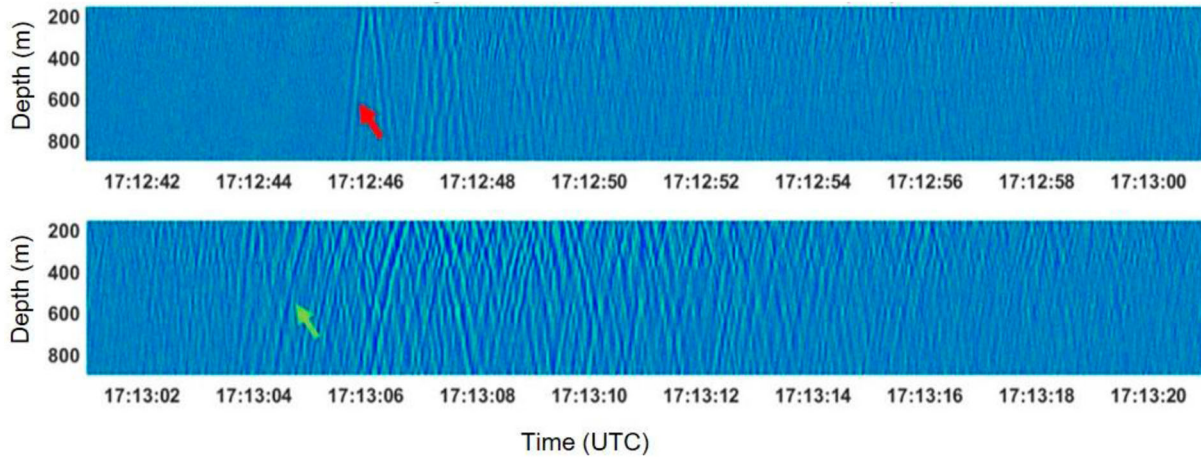


**Figure 2.** Raw DAS record of the  $M_L$  2.9 earthquake with an epicentre in Pingelly, Western Australia, happened on 5 June 2018 at 17:12:21 UTC. P- and S-wave arrivals are marked with red and green arrows, respectively.

generally also evident for local events (Figure 2). Such a prominent appearance of earthquakes enables their automatic identification. To this end, we first performed an automatic event detection using the semblance algorithm in a chosen velocity range. In particular: (i) we predefine apparent velocity range ( $v_{\min} = 1000$  m/s and  $v_{\max} = 6000$  m/s) and generate a set of velocities in this range with a spacing of 100 m/s, (ii) for each of the velocity from the above set, we apply normal move-out correction to the raw DAS data, (iii) we define the semblance window (5 s) that contains at least a few periods of signal oscillations for the lowest expected frequency of an event to be detected, (iv) for each velocity from the defined set, we calculate semblance in a sliding window, (v) we define velocity for which the semblance is the largest, and (vi) we compare this largest semblance value with a predefined threshold level (0.13), and if it is above the threshold, we record, in a text file, the apparent velocity corresponding to the largest semblance and the time when the semblance exceeded the threshold. Later, each of the selected events is examined and corrected manually. Since all the events are checked and corrected manually, we set the semblance threshold to a rather low value in order to not miss any of the events.

The identified events were cross-checked with earthquake data from the Geoscience Australia (GA) Database (2021). According to this database, the number of events detected worldwide during the experiment was 426. About 120 out of these 426 events happened in Australia, from which 52 events occurred in Western Australia and were detected with regional stations. The magnitudes of these 52 events vary from 1.6–4.7. The distance to the epicentre varies from 116 to 1700 km.

Over the duration of the observation, we recorded sixteen earthquakes: eight were local and eight were distant tremors. The distances to the earthquake epicentres vary from 126 km to 900 km for the local events and from 2300 km to 6400 km for the remote events (see Table 1).

**Table 1.** A list of earthquakes detected during the experiment.

Location	Distance to epicentre, km	Magnitude
Western Australia	126	2.9
Western Australia	141	1.9
Western Australia	225	3.1
Western Australia	250	2.9
Western Australia	550	3.4
Western Australia	558	4.3
Western Australia	558	4.7
Western Australia	900	4.3
Sumbawa region, Savu Sea	2550	5.1
Sumbawa region	2650	5.2
Sumbawa region	2650	5.3
South of Sumbawa region	2320	5.5
Sumbawa region	2650	5.5
South of Fiji	6400	5.6
Sumbawa region	2650	6.4
Sumbawa region	2700	6.4

The detectability of the earthquakes depends on the event magnitude and the distance to the epicentre from the sensor location. Thus, local event 2 (Table 1) with a minimal magnitude of 1.9 is only slightly above the detection limit.

The earthquake nearest to the well was detected on 5 June 2018 at 17:12:21 UTC with a magnitude of  $M_L$  2.9 (local magnitude) and the epicentre at Pingelly, Western Australia, 126 km east of Perth (Figure 2).

The axes in Figure 2 correspond to the UTC time (horizontal) and depth (vertical). The depth range 0–160 m is omitted due to a high level of surface wave noise. The P-wave arrival (marked with red arrow) is observed 24 s after the earthquake, followed by S-wave (marked with green arrow) 19 s later. The apparent velocities of the P- and S- waves measured along the well were 2744 and 1255 m/s, respectively.

Figure 3 shows an example of a local  $M_L$  3.1 Dumbleyung earthquake, which occurred 225 km away from the wellhead on 23 May 2018 at 17:26:55 UTC. The P- and S-waves were detected 41 and 72 s after the start of the earthquake, with apparent P and S-velocities of 2271 and 1144 m/s, respectively. Being 100 km further from the test well, the Dumbleyung earthquake has

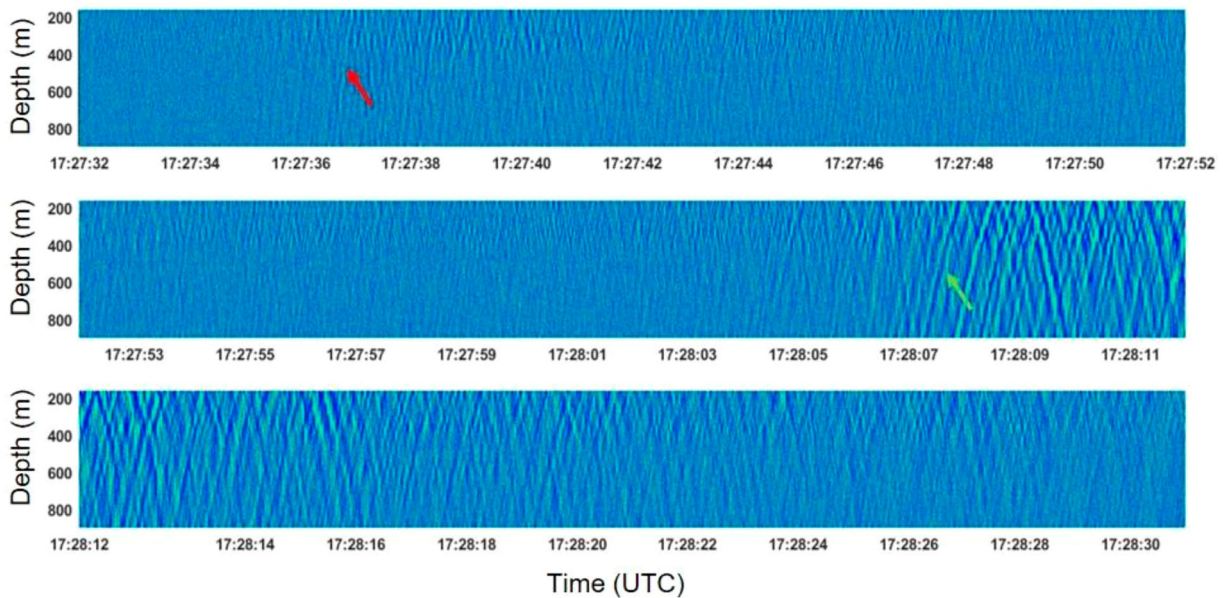


**Figure 3.** Raw DAS record of the ML 3.1 earthquake occurred in Dumbleyung, Wheatbelt Region, Western Australia, on 23 May 2018 at 17:26:55 UTC. P- and S-wave arrivals are marked with red and green arrows, respectively.

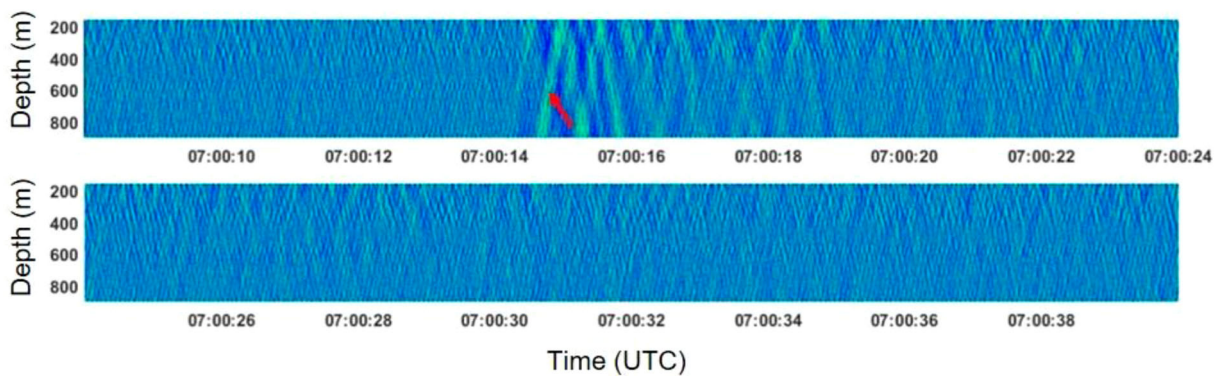


**Figure 4.** Raw DAS record of the  $M_D$  5.6 earthquake that occurred in the South of Fiji Islands on 12 July 2018 at 06:51:20 UTC. P-wave arrival is marked with a red arrow.

much weaker energy of the P-wave arrival. It also has a larger delay between P- and S-waves: 31 s vs. 19 s and a lower frequency content of the S-wave: central frequency of 4.3 Hz vs. 7.8 Hz. The P-wave frequency was around 7 Hz for both earthquakes.

The most distant event we recorded was an earthquake with a body-wave magnitude  $M_b$  5.6 in the South of Fiji Islands, about 6413 km away from the well on 12 July 2018 at 06:51:20 UTC (Figure 4). The P-wave is detected 8 min 54 s after the onset of the earthquake tremor. For this remote event, no S-wave is detectable, probably due to attenuation over such a long distance or low sensitivity of DAS waves polarised perpendicular to the fibre.

The minimal detectable magnitude we recorded during the experiment was  $M_L$  1.9, corresponding to an earthquake that occurred in Quairading, Western Australia, 141 km east of the research site. The earthquake with the largest magnitude of 6.4  $M_w$  (moment magnitude) came from Sumbawa, Indonesia, 2583 km to the north on 28 July 2018 at 22:47:39 (Figure 5), which

shows the P-wave arrival at  $\sim$  22:53:10 (marked with a red arrow) and S-wave arrival at 22:57:18 (marked with a green arrow), 5 min 31 s and 9 min 39 s after the start of the earthquake, respectively.

The mean frequency of the P-wave measured on the records varies from 2 Hz for the remote events to 12–14 Hz for local earthquakes (Figure 6).

### **Blasting at local mine sites (within $\sim$ 100 km)**

Over the experiment time, we have also recorded fifty-five seismic events that did not appear in the earthquake database. These events were identified by the automatic event detection algorithm based on the semblance analysis. Each event appeared on the data as a set of two up-going waves corresponding to P- and SV-wave arrivals. The signature of these events is similar to that of the earthquake pattern but with a higher frequency content and a smaller interval between P- to S-wave arrivals compared to the earthquakes. The regularity of these events, similar initiation times of the day

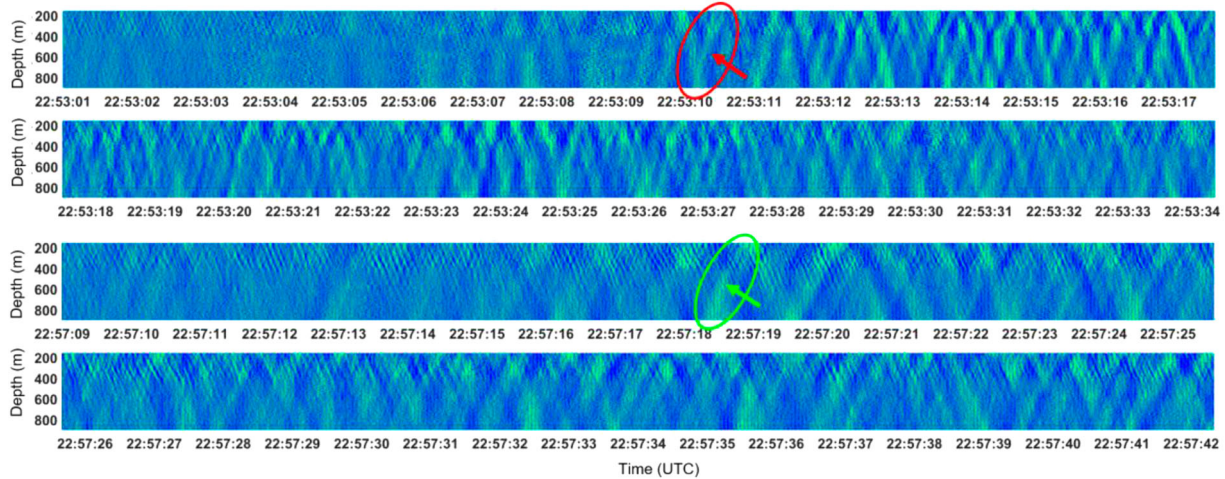


**Figure 5.** Raw DAS record of the 6.9 Mwp earthquake in Sumbawa Region, Indonesia, happened on 28 July 2018 at 22:47:39. P- and S-wave arrivals are marked with red and green arrows, respectively.

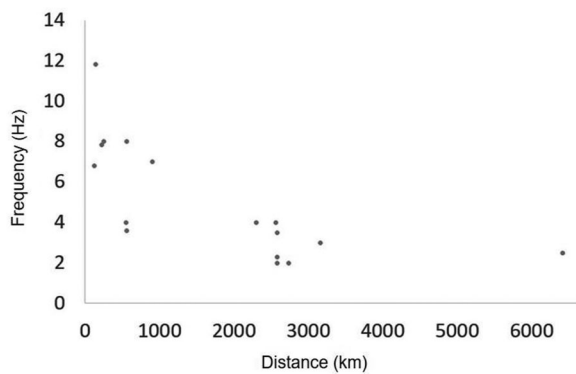


**Figure 6.** Dominant frequency of P-wave arrivals versus the distance to the earthquake epicentre.

as well as proximity to mining site locations suggests that these events likely correspond to human activity, namely mine blasting.

Figure 7 shows a typical example of such an event that happened on 5 June 2018 at 04:52:39 UTC. The time difference between P and S waves (marked red and green arrows, respectively) arrivals suggests that this event was initiated  $\sim 25$  km away from the testing well. The possible epicentre may be a quarry located at 25-km radius mark.

The average apparent P- and S-wave velocities for the events related to the blasting are 2700 and

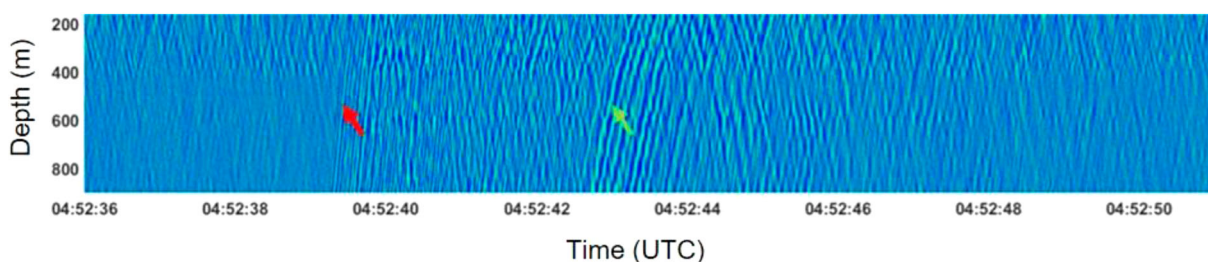
1300 m/s, respectively. The frequency contents of the P- and S-waves are similar and vary from 5 to 25 Hz, see Figure 8.

Interestingly, the times of the day for the P-wave arrivals are quite regular and mostly correspond to afternoon hours (Figure 9), which correlates with the scheduled blasting times.

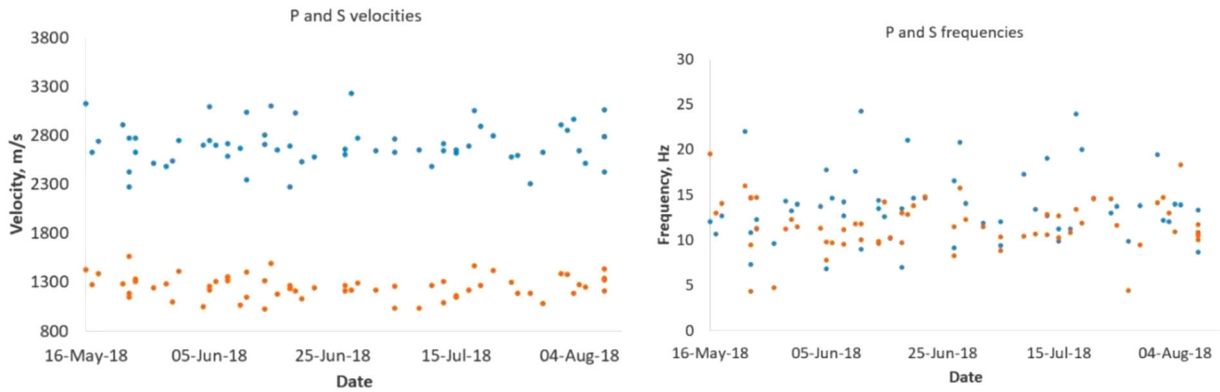
The time delay between P- and S-waves ( $\Delta T$ ) provides an estimate of the distance to an epicentre ( $D$ ), which can be calculated as  $D = \Delta T \cdot \text{coefficient}$ . The coefficient  $V_p \cdot V_s / (V_p - V_s)$  was estimated analytically based on the earthquakes data taken from the GA Earthquakes database, namely distances to the epicentres and the earthquakes' incidence times. The corresponding P- and S-wave arrival times found in the recorded DAS data for the selected earthquakes provided time delay estimations ( $\Delta T$ ). We plot the distances ( $D$ ) versus the time delays ( $\Delta T$ ). The coefficient  $D = 7.5$  was then estimated from a linear fit.

Figure 10 shows a map with the marked well location in the centre and the local mining sites within 100-km radius. Table 2 shows the local mine site names, distances to the sites from the well and expected time delays between P- and S-waves.

Having this image in mind, the fifty-five recorded events were further conditionally classified into five groups based on the time delay between P- and S-wave



**Figure 7.** Raw DAS record showing the mine site blasting at a quarry 25 km away from the site. P- and S-wave arrivals are marked with red and green arrows, respectively.



**Figure 8.** P-wave (blue) and S-wave (orange) average apparent velocities (left) and mean frequencies (right) for the events related to the mine site blasting.

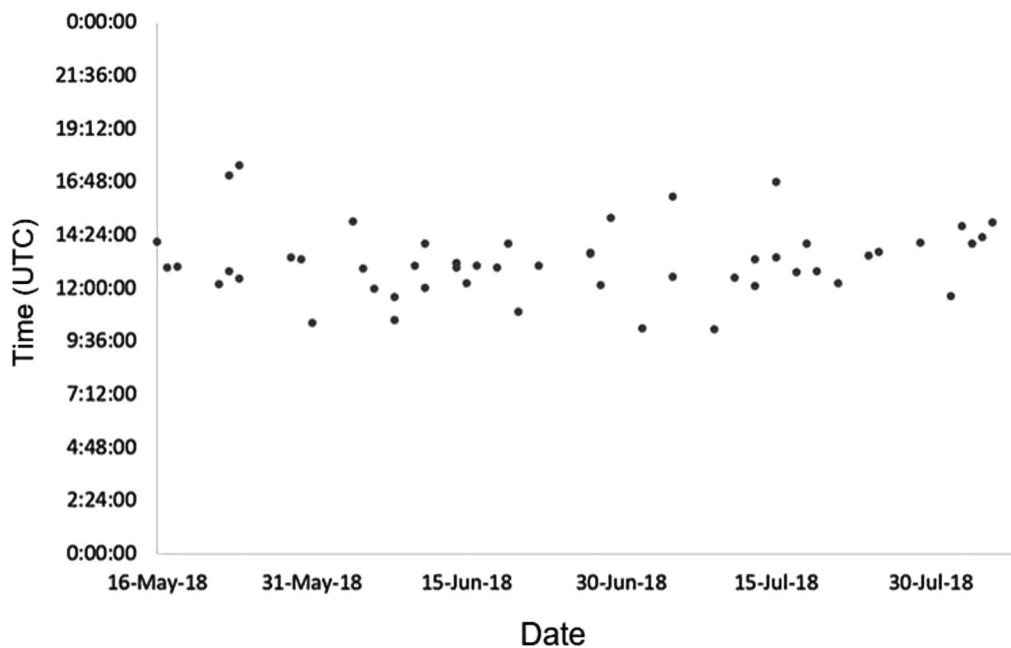


**Figure 9.** Time of P-wave arrivals for the events related to the mine blasting.

arrivals, ranging from 2.3-s (coming from a quarry  $\sim$  25 km away from the well) to 14.7-s delay (mining at  $\sim$  100 km away) (Figure 11). The groups are marked with different colours: light blue (time delays ranging 2–5 s), orange (5.5–7.5 s), grey (8.4–10.65 s), yellow (11.3–11.95 s) and blue (12–15 s).

### **Traffic, local noise and machinery**

We also closely analysed traffic, local machinery noise on seismograms and spectrograms. The presence of the urban noise is evident in the shallow part of the data up to the depth of 160 m (see Figure 12). Figure 12 demonstrates the DAS recordings of an earthquake (same as in Figure 2) in a range of the depths starting from 0 m (top image) and the same recording with a muted shallow part of the data from 0 to 160 m (bottom image). Note the high energy level of the urban noise in the shallow part (top image) and its effect on visibility of the data 160–900 m (bottom image). In other examples, the top

part of the data was excluded from the analysis of earthquakes and mine blasting events in order to enhance their visibility. See the improvement in its prominence and overall visibility of the P-wave arrival (generated by the earthquake 126 km away from the well and marked with red arrows) in the bottom image when compared to the top one.

Human-generated events are observed as down-going waves with a negative slope on a seismic record (arrival time increasing with depth) (Figure 13).

The event detection algorithm based on the semblance analysis captured more than 200 such events for each day over the observation period, totalling more than 17,000 events and making it challenging to use them for further analysis. As such, the intensity of these occasions and the overall pattern can be better visualised using spectrograms.

Figure 14 shows a spectrogram recorded at a depth of 250 m on 20 May 2018. Here, we can clearly see the decrease in the intensity during the night-time (from

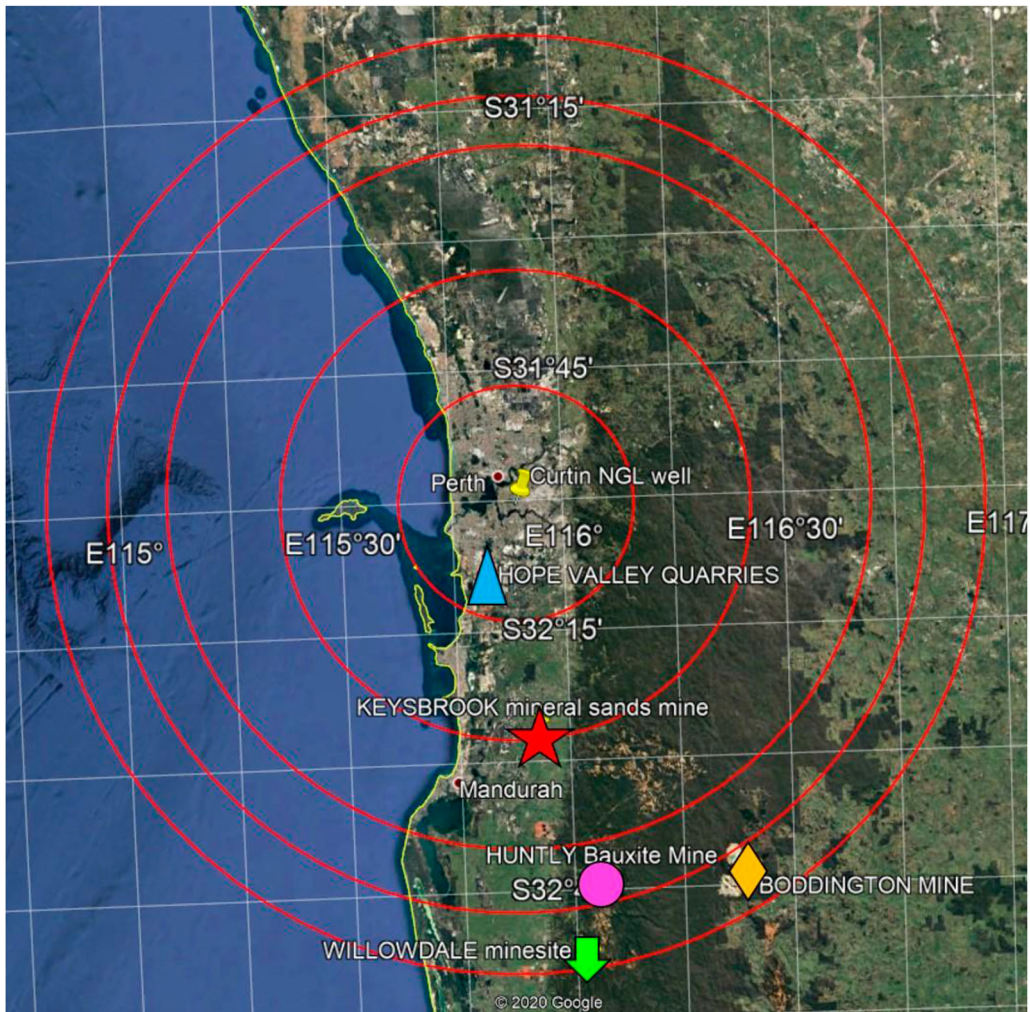


**Figure 10.** A map showing well location in the centre and local mining sites within 100 km radius. The red circles have radii of 25, 50, 75, 87 and 100 km.

**Table 2.** Local mine sites, the distances from the NGL well and approximate expected time delays between P- and S-waves.

Mine site	Km	Time delay, s	Marker
Hope Valley	23	3.1	
Keysbrook	52	6.9	
Huntly	85	11.3	
Boddington	95	12.7	
Willowdale	101	13.5	

midnight to 7.30 AM and from 9 PM). The data analysis shows a number of mono-frequency events mainly ranging from 2 Hz up to 50 Hz. There are a number of continuous events, which exist everywhere at all times and have a frequency around 17.5 Hz; several events with a frequency of 4 Hz, which only appear during office hours on the weekdays; some events appear on the record only occasionally. All these occasions are most likely attributed to various running equipment and machinery around the site. For example, the 14 Hz event is day- and time-dependent. It disappears at

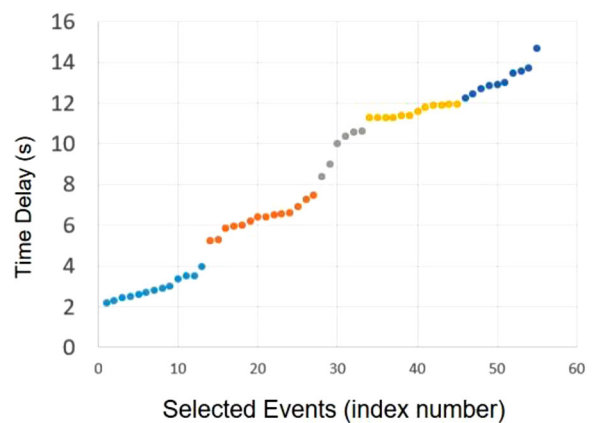


**Figure 11.** Event classification based on the time delay between P- and S-wave arrivals.

around 6:15 PM on Fridays and then appears at various times on Mondays. The 4.88 Hz event is present during working hours only on weekdays from 7:15 AM until 4:30 PM and sometimes subsides around lunchtime.

Figure 15 shows a behaviour of the 22-Hz component on the spectrograms of two consecutive days on 29–30 June 2018 as observed at a depth of 250 m.

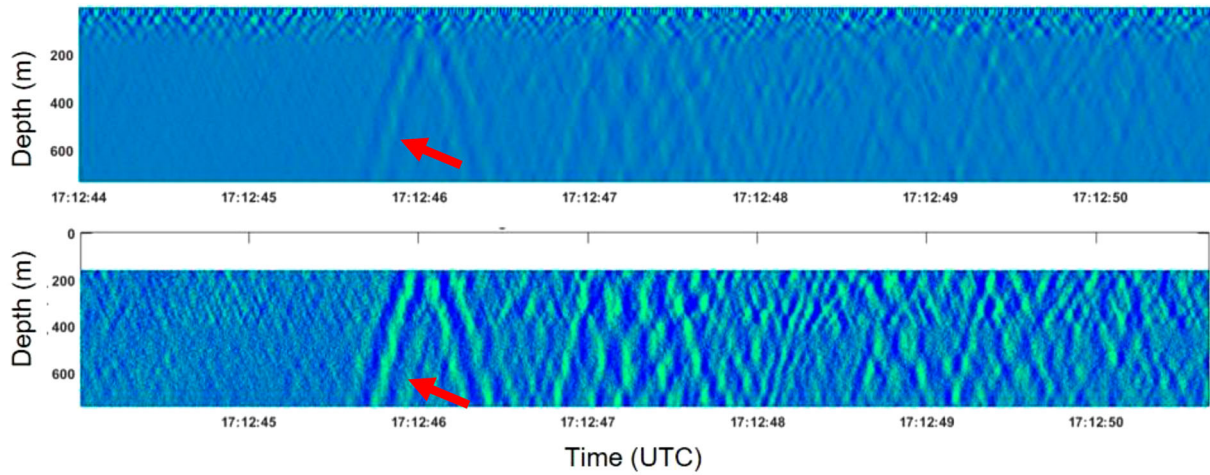


**Figure 12.** A fragment of the same raw DAS record in a depth range starting from 0 m (top image) and with a muted shallow part of the data (0–160 m) (bottom image).

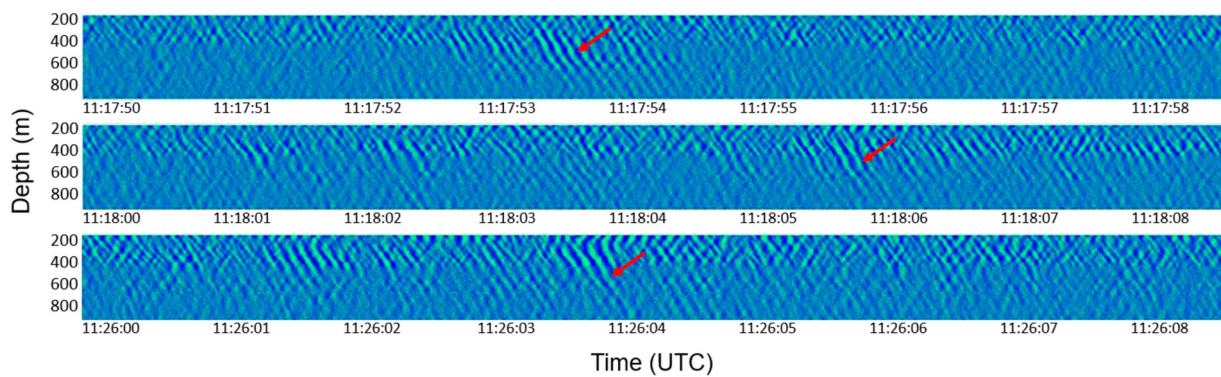


**Figure 13.** Raw DAS record showing down-going waves (marked with red arrows) related to the human activities in the vicinity of the well.

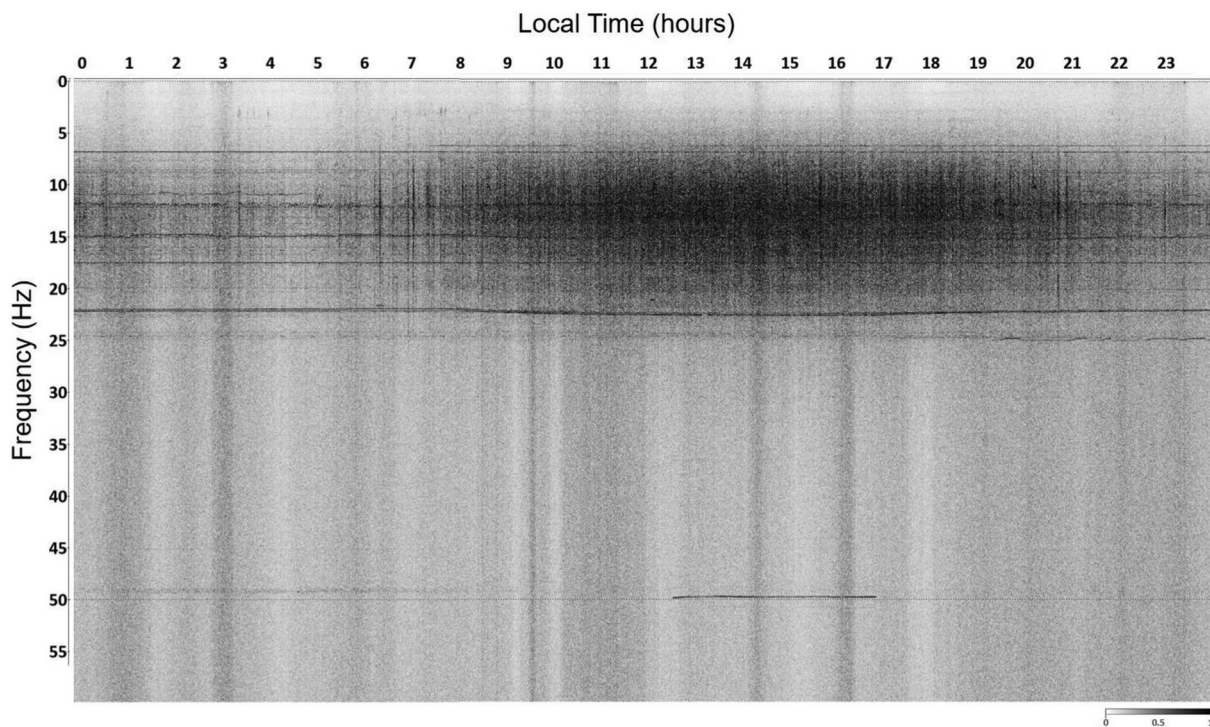


**Figure 14.** Spectrogram computed at the depth of 250 m on 20 May 2018.

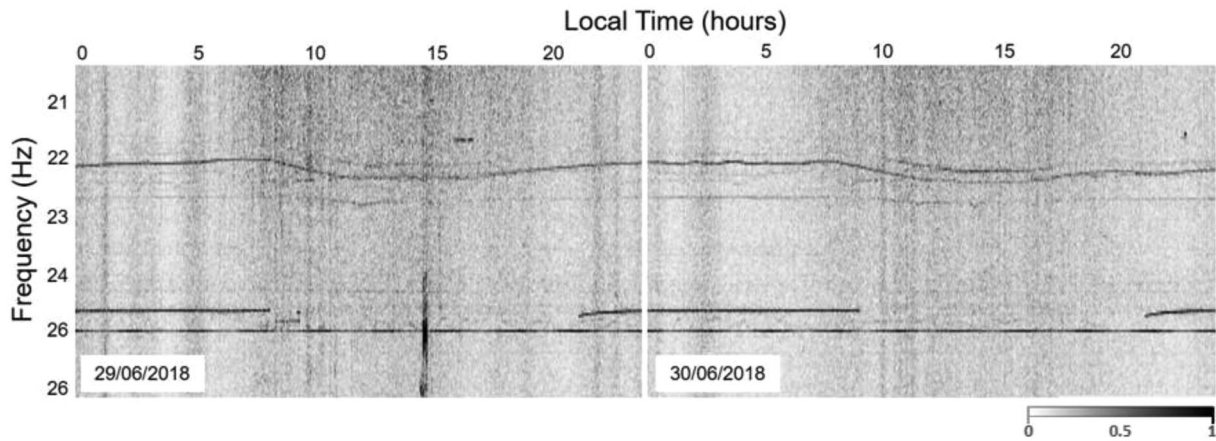


**Figure 15.** Behaviour of  $\sim 22$  Hz component on the spectrograms computed at the depth of 250 m on 29–30 June 2018.

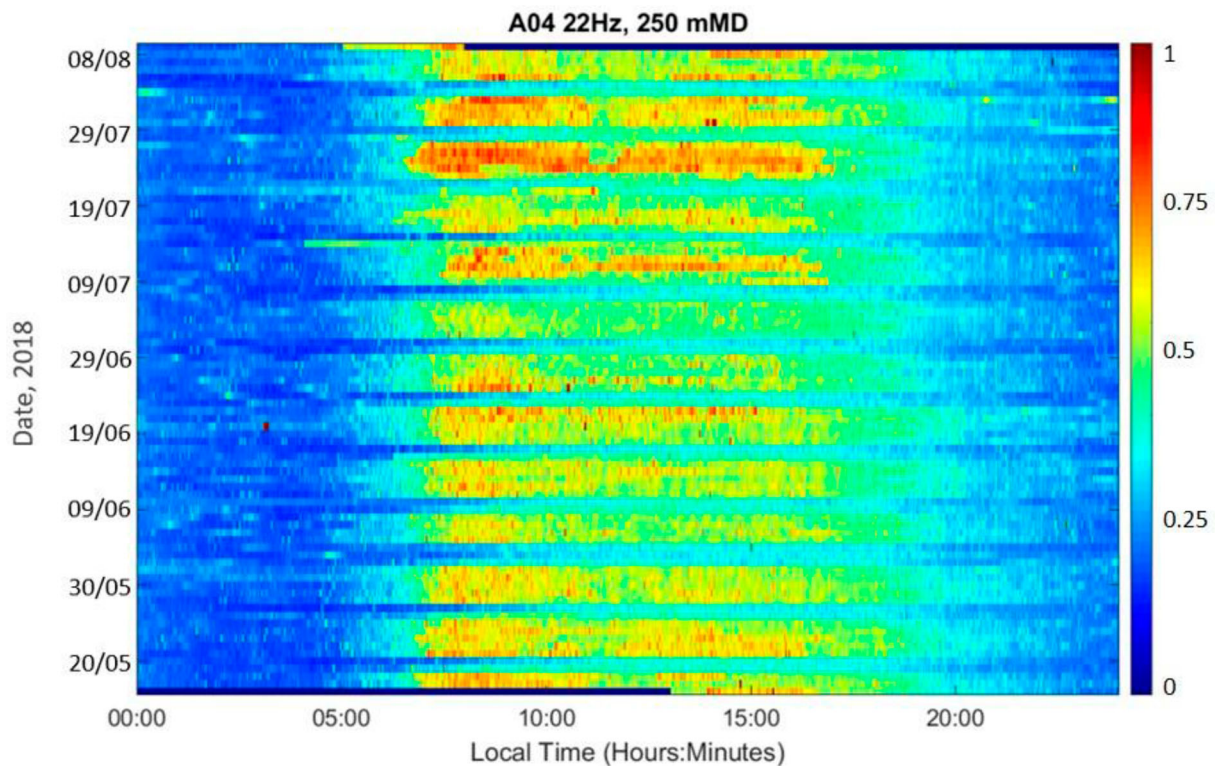


**Figure 16.** Amplitude distribution in 4–22 Hz frequency range at 250 m depth over time.

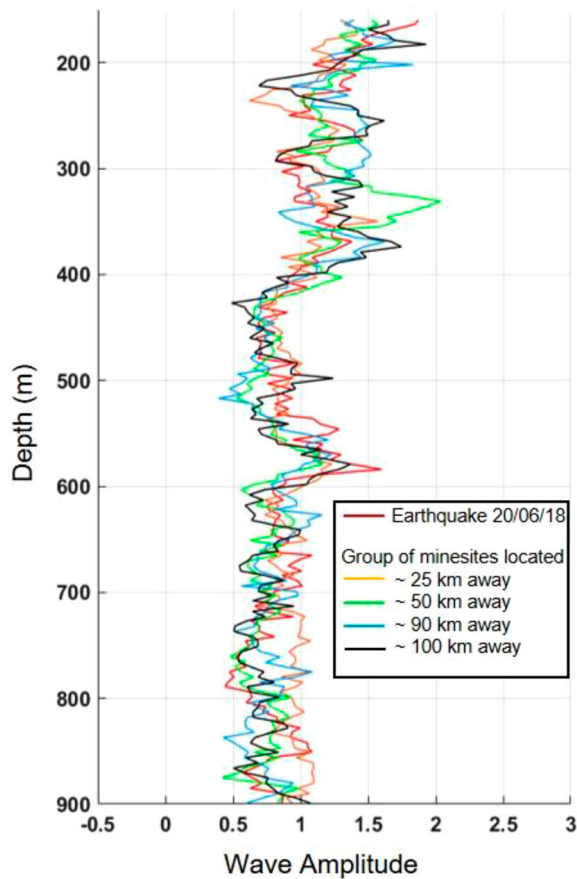
A 22 Hz-event experiences a gradual increase in the morning hours around 8 AM, has its peak at about 2 PM, and then decreases again. This event may be related to an air-conditioning system and its increasing operational intensity due to a daytime natural heating of a nearby office.

Figure 16 shows the amplitude distribution in 4–22 Hz frequency range at 250-m depth (single channel) for the whole duration of the experiment from 16 May till 9 August 2018. The axes correspond to the UTC time (horizontal) and the date (vertical). The amplitude changes (shown by colour) demonstrate the overall pattern of local events related to human activity, which increases during daytime (green, yellow and red colours) and subsides at night-time (blue). The blue horizontal stripes correspond to weekends. The local

increase in the width of the stripe on 4 June 2018 corresponds to a long weekend. The relative decrease in the intensity at around 28 June–8 July 2018 may be related to the first week of school holidays.

Pevzner et al. (2020) showed that as a P-wave arrival of relatively distant earthquake can be treated as a plane wave, the inverse amplitude should be proportional to  $(\rho V_p^3)^{1/2}$ , where  $\rho$  is density and  $V_p$  is the P-wave velocity. As such, we can use P-wave amplitudes of these earthquakes to derive a “well log” containing information about the distribution along the well, and, potentially, temporal variation of the elastic properties. However, in that study, only two relatively strong events recorded in the same well were analysed.

To build upon the analysis of Pevzner et al. (2020), we compare amplitudes recorded during the experiment



**Figure 17.** Comparison of the RMS normalised amplitudes of recorded P-waves for the earthquake (red) and 4 local blasts from different locations.

of the natural events, i.e. earthquake, against those of human-related events, such as blasting. Figure 17 shows a comparison of the RMS normalised amplitudes of the recorded upgoing P-waves for the earthquake (red) and four local mine sites from different locations (orange  $\sim 25$  km away from the well), green ( $\sim 50$  km), blue ( $\sim 90$  km) and black ( $\sim 100$  km). Note that all the lines show similar trends.

### Surface waves generated by the ocean waves and swell

The well is located only about 13 km away from the Indian Ocean coast. As such, we can expect the ocean swell to appear on the recordings (see e.g. Glubokovskikh et al. 2020). Figure 18 shows a comparison of the spectrograms (left) and their amplitude spectra (right) computed at various depths for the recording of 21 July 2018. The horizontal axis is time in hours, and the vertical axis is data frequency in Hz. The greyscale shows the amplitude intensity. The ocean swell within a frequency range of 0.5–0.8 Hz appears on the data persistently (see Figure 18, left). The ocean swell could be detected in the spectrograms at depths down to 202 m. The depth of 236 m is probably a borderline for the detection of these events (see Figure 18, right).

Figure 19 shows amplitude distribution in 0.2–0.9 Hz frequency range at 250 m depth (blue plot) overlaid with wind speed recordings (orange plot) taken at local WA stations (Australian Bureau of Meteorology).

Both curves show overall similarity along the whole duration of the experiment. Note the correspondence between the peaks around 25 May, 4 June and 23 July 2018 related to big storms.

## Discussion

The location of the test well drilled in urban settings relatively close to the ocean coast enables the recording of seismic energy from various sources of natural and human origin. This paper has focused on the identification of these sources on passive DAS records, similar to the forensic seismology approach. The analysis of passive data collected with DAS in this well demonstrates that elastic waves can be detected at any depth from the surface to the bottom of the well.

While, in principle, DAS can be used from mHz range (e.g. Parker, Shatalin, and Farhadiroushan 2014; Becker et al. 2017), in this experiment, the lowest detectable signal (ocean swell) was above 0.1 Hz (Figure 18). We attribute this to specific features of the interrogator design and the choice of acquisition parameters as both Parker, Shatalin, and Farhadiroushan (2014) and Becker et al. (2017) used a different DAS interrogator (iDASv2, Silixa). Having frequencies below 0.1 Hz in the record may be beneficial for the analysis of global planetary processes, such as Earth tides.

Above 0.1 Hz, DAS sensitivity is high enough to record a large variety of events that might be of interest for various applications. The analysis of urban noise can provide an abundance of information about human activities. For example, in our experiment, we were able to detect on and off times of machinery and their level of noise even from the downhole fibre placed in a vertical well (Figure 14). Even though we were not able to locate the machinery source, the spectrograms derived from the DAS data provided overall characteristics of the urban noise field, their intensity, frequency content and activity times. Unlike the passive seismic data acquired in quiet rural environments, data from the city provide information about properties and vertical distribution of the urban noise. It gives an opportunity to both study human activities and use this information to understand the limitations on which natural processes can be studied in such environments. It is important to emphasise that the urban noise can be detected over the entire depth of the well; e.g. there is no such depth in the well where the noise will drop below DAS sensitivity.

The DAS data also contained a number of events related to mine blasting. The correlation of the recorded events with a list of existing mine sites shows that we can detect activities on the mine sites located as far as 100 km over the entire length of the borehole.

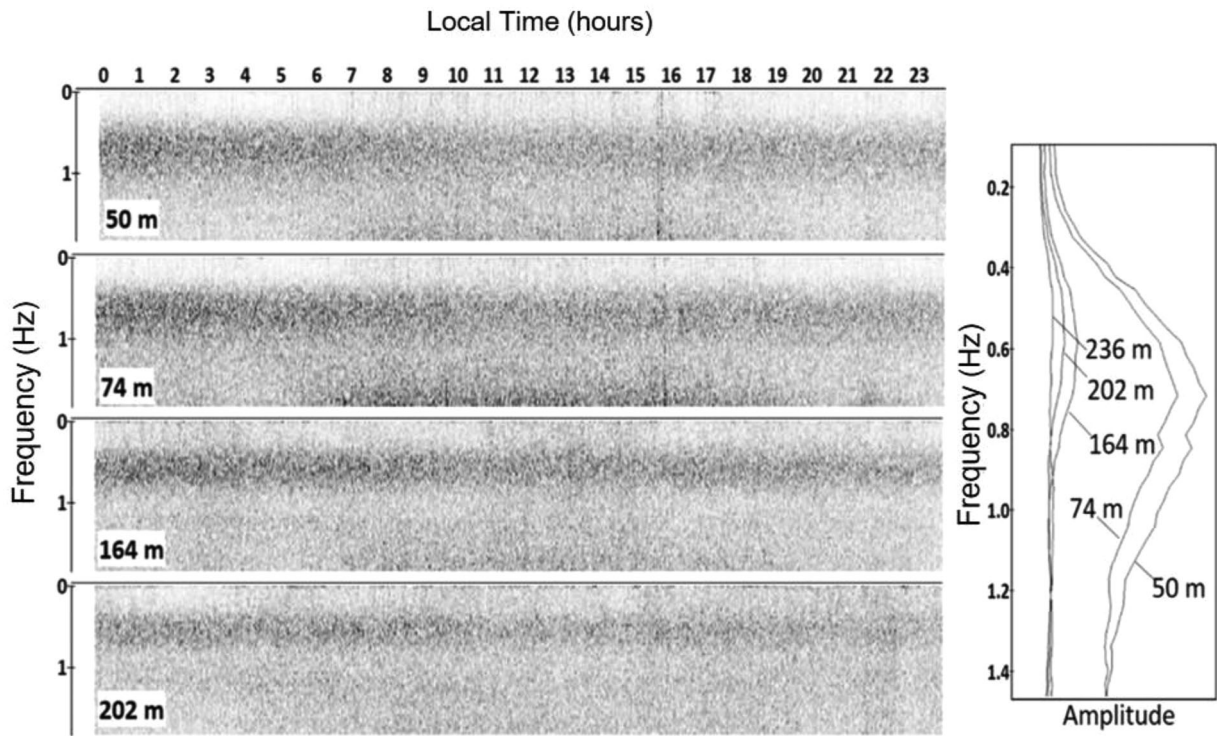


**Figure 18.** Comparison of the spectrograms (left) and their amplitude spectra (right) computed at various depths for the recording of 21 July 2018.

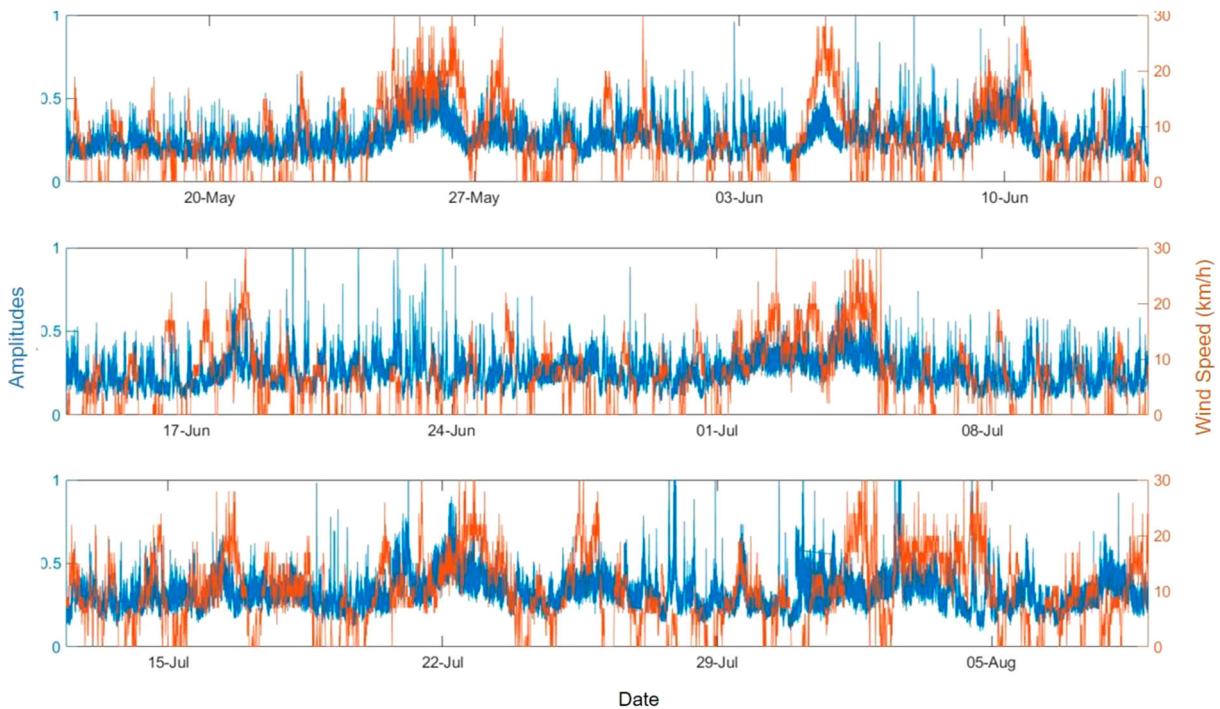


**Figure 19.** Amplitude distribution in 0.2–0.9 Hz frequency range at the 250 m depth (blue plot) overlaid with wind speed recordings (orange plot) for the whole duration of the experiment.

Natural seismic events detected on DAS data primarily include earthquakes and ocean swell. Amplitudes of earthquakes recorded by DAS can be used to derive the distribution of the elastic properties along the well. The similarity of the plots in Figure 17 derived for both an earthquake and several blasting events confirms that, in principle, mine blasts can be utilised for this purpose too. However, the degree of repeatability of the

measurement is affected by the presence of the other urban noise, and further studies are required to optimise the amplitude analysis.

If the main goal is to detect earthquakes or blasting events detection, then the main limitation would be the presence of urban noise (up to 160-m range, Figure 12) and depth of the well, but not the DAS sensitivity. In this case, a way to overcome these issues is to use DAS

sensors placed in a quiet (e.g. rural) environment, which provides even higher clarity of the data.

The earthquake/blasting monitoring may be further enriched with a simultaneous recording by an array of several wells separated by tens, hundreds or thousands of kilometres. Regional or even global versus single well approach might be potentially adopted in seismology.

Despite the fact that each point on the sensing fibre is equivalent to a single-component seismic sensor, the ability to analyse travel time curves partially compensates for the absence of three-component geophones. In particular, our analysis shows that the slope of the travel-time curve can differentiate downward going waves from upward going ones and P- from S-waves. Moreover, since different events have different apparent P- and S-wave velocities along the well, it is possible to infer some information about the angle at which a particular seismic wave crosses the well. In this respect, simultaneous recording in several wells separated by a few kilometres opens additional opportunities for underground characterisation using ambient noise.

The energy from natural processes such as ocean swell can also be observed on the downhole DAS data. It appears in a low-frequency range of the data (Figure 18). In fact, even at a depth as large as 250 m, there is a strong correlation between the level of noise and wind speed (Figure 19) and associated wind waves and swell. Interestingly, there is sometimes a time shift between the wind and swell noise in curves around 19 June, 17 and 22 July with high wind speed delayed by up to one day. This can happen if the swell from a distant weather event came ahead of strong winds (Glubokovskikh et al. 2020).

The link between low-frequency Raleigh waves and wind provides an opportunity to use downhole data, i.e. a well instrumented with the DAS fibre, for global earth physics, including sea and atmospheric processes (e.g. wave climate from oceanic microseisms (Glubokovskikh et al. 2020), infrasound related to distant explosions or fireballs (NORSAR 2021. <https://t.co/gai6DCFJlv?amp=1>)).

## Conclusions

Analysis of 85 days of continuous passive DAS record from a 900-m deep well located at the Curtin University campus in Perth, Australia, demonstrates that ambient elastic energy in a form of both surface and body waves can be detected at any depth, from surface to the bottom of the well. This was done using a conventional single-mode fibre in a cable cemented behind the casing of the well.

Dominant sources of energy comprise oceanic microseisms, human-related events including both vehicle traffic and mine site blastings as well as natural seismicity. We detected 16 regional earthquakes and teleseismic events and 55 blasting events from distances of up

to ~ 100 km. Both earthquakes and mine blasts can be used to characterise the vicinity of the well.

DAS appears to be sufficiently sensitive for global seismology applications. The lack of polarisation analysis can be compensated by the multi-channel nature of DAS sensors, which gives travel-time curves for each event.

The urban location of the NGL facility allowed us to explore the relationship between the noise levels and the local traffic activity. However, this traffic noise is present at any depth, which complicates the analysis of ambient seismic energy linked to other sources. As such, it may be useful to compare the records from this well and a well located in a quiet environment.

## Acknowledgements

The authors acknowledge the support provided by the Commonwealth Scientific and Industrial Research Organization (CSIRO), Australia. The support of the sponsors of the Curtin Reservoir Geophysics Consortium (CRGC) is also gratefully acknowledged.

## Disclosure statement

No potential conflict of interest was reported by the author(s).

## ORCID

Konstantin Tertyshnikov  <http://orcid.org/0000-0002-8456-7391>

Roman Pevzner  <http://orcid.org/0000-0002-2555-6860>

Boris Gurevich  <http://orcid.org/0000-0002-2752-3528>

## References

- Ajo-Franklin, J.B., S. Dou, N.J. Lindsey, I. Monga, C. Tracy, and M. Robertson. 2019. Distributed acoustic sensing using dark fiber for near-surface characterization and broadband seismic event detection. *Scientific Reports* 9 no. 1: 1–14.
- Alfataierge, E., A. Ali Aldawood, A. Bakulin, R.R. Stewart, and H. Merry. 2020. Influence of gauge length on DAS VSP data at the Houston research center test well. *90th Annual International Meeting, SEG, Expanded Abstracts*, 505–509. doi:10.1190/segam2020-3419066.1
- Becker, M.W., C. Ciervo, M. Cole, T. Coleman, and M. Mondanos. 2017. Fracture hydromechanical response measured by fiber optic distributed acoustic sensing at milliHertz frequencies. *Geophysical Research Letters* 44: 7295–7302.
- Biondi, B., E. Martin, S. Cole, and M. Karrenbach. 2017. *Earthquakes analysis using data recorded by the Stanford DAS Array: Stanford Exploration Project*, Report 168, 11–26.
- Daley, T., B. Freifeld, J. Ajo-Franklin, S. Dou, R. Pevzner, V. Shulakova, S. Kashikar, et al. 2013. Field testing of fiber-optic distributed acoustic sensing (DAS) for subsurface seismic monitoring. *The Leading Edge* 32: 699–706.
- Dou, S., N. Lindsey, A.M. Wagner, T.M. Daley, B. Freifeld, and M. Robertson. 2017. Distributed acoustic sensing for seismic monitoring of the near surface: A traffic-noise interferometry case study. *Scientific Reports* 7 no. 1: 1–12.
- Geoscience Australia Earthquakes Database. 2021. <https://earthquakes.ga.gov.au/>.

- Glubokovskikh, S., R. Pevzner, E. Sidenko, K. Tertyshnikov, B. Gurevich, S. Shatalin, A. Slunyaev, and E. Pelinovsky. 2020. Downhole distributed acoustic sensing reveals the wavefield structure of the coastal microseisms. *Submitted to Earth and Planetary Science Letters*. doi:10.31223/X5W30H.
- Glubokovskikh, S., R. Pevzner, E. Sidenko, K. Tertyshnikov, B. Gurevich, S. Shatalin, et al. 2021. Downhole distributed acoustic sensing provides insights into the structure of short-period ocean-generated seismic wavefield. *Journal of Geophysical Research: Solid Earth* 126: e2020JB021463. doi:10.1029/2020JB021463.
- Hartog, A.H. 2017. *An introduction to distributed optical fiber sensors*. CRC Press. doi:10.1201/9781315119014
- Hartog, A.H. 2020. Distributed sensors in the oil and gas industry. In *Optical fiber sensors*, eds. I del Villar, and I.R. Matias, 151–191. Hoboken: John Wiley & Sons.
- Hudson, T.S., A.F. Baird, J.M. Kendall, S.K. Kufner, A.M. Brisbane, A.M. Smith, A. Butcher, et al. 2021. Distributed acoustic sensing (DAS) for natural microseismicity studies: A case study from Antarctica. *Journal of Geophysical Research: Solid Earth* 126: e2020JB021493.
- Issa, N.A., D. Lumley, and R. Pevzner. 2017. Passive seismic imaging at reservoir depths using ambient seismic noise recorded at the Otway CO2 geological storage research facility. *Geophysical Journal International* 209: 1622–1628.
- Lellouch, A., and B.L. Biondi. 2021. Seismic applications of downhole DAS. *Sensors* 21: 2897. doi:10.3390/s21092897.
- Lellouch, A., R. Schultz, N.J. Lindsey, B.L. Biondi, and W.L. Ellsworth. 2021. Low-magnitude seismicity with a downhole distributed acoustic sensing array – examples from the FORGE geothermal experiment. *Journal of Geophysical Research: Solid Earth* 126: e2020JB020462.
- Lellouch, A., S. Yuan, W.L. Ellsworth, and B. Biondi. 2019a. Velocity-based earthquake detection using downhole distributed acoustic sensing – examples from the San Andreas Fault Observatory at depth. *Bulletin of the Seismological Society of America* 109 no. 6: 2491–2500.
- Lellouch, A., S. Yuan, Z. Spica, B. Biondi, and W.L. Ellsworth. 2019b. Seismic velocity estimation using passive downhole distributed acoustic sensing records: examples from the San Andreas fault observatory at depth. *Journal of Geophysical Research: Solid Earth* 124 no. 7: 6931–6948.
- Lindsey, N.J., and R. Martin Eileen. 2021. Fiber-optic seismology. *Annual Review of Earth and Planetary Sciences* 49 no. 1, 309–336.
- Lindsey, N.J., R. Martin Eileen, S. Dreger Douglas, F. Barry, C. Stephen, R. James Stephanie, B.L. Biondi, et al. 2017. Fiber-optic network observations of earthquake wavefields. *Geophysical Research Letters* 44: 11–792.
- Martin, E., N. Lindsey, S. Dou, J. Ajo-Franklin, T. Daley, B. Freifeld, M. Robertson, C. Ulrich, A. Wagner, and K. Bjella. 2016. Interferometry of a roadside DAS array in fairbanks, AK. *SEG Technical Program Expanded Abstracts*, 2725–2729. doi:10.1190/segam2016-13963708.1
- Martin, E.R., and B.L. Biondi. 2018. Eighteen months of continuous near-surface monitoring with DAS data collected under Stanford university. *SEG Technical Program Expanded Abstracts 2018*, 4958–4962.
- Martin, E.R., B.L. Biondi, S. Cole, and M. Karrenbach. 2017a. *Overview of the Stanford DAS Array-1 (SDASA-1), Stanford Exploration Project*, Report 168.
- Martin, E.R., B.L. Biondi, M. Karrenbach, and S. Cole. 2017b. Ambient noise interferometry from DAS array in underground telecommunications conduits. *79th EAGE Conference and Exhibition 2017*, 1–5.
- Martin, E.R., C.M. Castillo, S. Cole, P.S. Sawasdee, S. Yuan, R. Clapp, M. Karrenbach, and B.L. Biondi. 2017. Seismic monitoring leveraging existing telecom infrastructure at the SDASA: active, passive, and ambient-noise analysis. *The Leading Edge* 36: 1025–1031.
- Mateeua, A., J. Mestayer, B. Cox, D. Kiyashchenko, P. Wills, J. Lopez, S. Grandi, et al. 2012. Advances in distributed acoustic sensing (DAS) for VSP. *SEG Technical Program Expanded Abstracts*, 1–5.
- Mestayer, J., B. Cox, P. Wills, D. Kiyashchenko, J. Lopez, M. Costello, S. Bourne, et al. 2011. Field trials of distributed acoustic sensing for geophysical monitoring. *SEG Technical Program Expanded Abstracts*, 4253–4257.
- Mondanos, M., and T. Coleman. 2019. Application of distributed fiber-optic sensing to geothermal reservoir characterization and monitoring. *First Break* 37: 51–56.
- NORSAR on LinkedIn. 2021. <https://t.co/gai6DCFjLv?amp=1>.
- Parker, T., S. Shatalin, and M. Farhadiroushan. 2014. Distributed acoustic sensing – a new tool for seismic applications. *First Break* 32: 61–69.
- Pevzner, R., B. Gurevich, A. Pirogova, K. Tertyshnikov, and S. Glubokovskikh. 2020. Repeat well logging using earthquake wave amplitudes measured by distributed acoustic sensors. *The Leading Edge* 39: 513–517.
- Pevzner, R., K. Tertyshnikov, and A. Bona. 2018. Feasibility of passive vertical seismic profiling using distributed acoustic sensing for monitoring applications. *80th EAGE Conference & Exhibition 2018* 1: 1–5.
- Richter, P., T. Parker, C. Woerpel, Y. Wu, R. Rufino, and M. Farhadiroushan. 2019. Hydraulic fracture monitoring and optimization in unconventional completions using a high-resolution engineered fiber-optic distributed acoustic sensor. *First Break* 37: 63–68.
- Shen, J., and T. Zhu. 2021. Seismic noise recorded by telecommunication fiber optics reveals the impact of COVID-19 measures on human activity. *The Seismic Record* 1: 46–55.
- Shragge, J., J. Yang, N. Issa, M. Roelens, M. Dentith, and S. Schediwy. 2019. Low-frequency ambient distributed acoustic sensing (DAS): useful for subsurface investigation? *SEG Technical Program Expanded Abstracts*, 963–967.
- Spica, Z.J., M. Perton, E.R. Martin, G.C. Beroza, and B. Biondi. 2020. Urban seismic site characterization by fiber-optic seismology. *Journal of Geophysical Research: Solid Earth* 125 no. 3: 1–14.
- Verdon, J.P., S.A. Horne, A. Clarke, A.L. Stork, A.F. Baird, and J.-M. Kendall. 2020. Microseismic monitoring using a fiber-optic distributed acoustic sensor (DAS) array. *Geophysics* 85 no. 3: 1–48.
- Walter, F., D. Gräff, F. Lindner, P. Paitz, M. Köpfli, M. Chmiel, and A. Fichtner. 2020. Distributed acoustic sensing of microseismic sources and wave propagation in glaciated terrain. *Nature Communications* 53 no. 9: 1689–1699.
- Wang, H.F., X. Zeng, D.E. Miller, D. Fratta, K.L. Feigl, C.H. Thurber, and R.J. Mellors. 2018. Ground motion response to an ML 4.3 earthquake using co-located distributed acoustic sensing and seismometer arrays. *Geophysical Journal International* 213 no. 3: 2020–2036.
- Williams, E.F., M.R. Fernández-Ruiz, R. Magalhaes, R. Vanthillo, Z. Zhan, M. González-Herráez, and H.F. Martins. 2019. Distributed sensing of microseisms and teleseisms with submarine dark fibers. *Nature Communications* 10: 1–11.
- Yu, C., Z. Zhan, N.J. Lindsey, J.B. Ajo-Franklin, and M. Robertson. 2019. The potential of DAS in teleseismic studies: insights from the goldstone experiment. *Geophysical Research Letters* 46: 1320–1328.